15th Canadian Masonry Symposium
Ottawa, Canada
June 2-5, 2025

From Monitoring to Modeling: 3D-DEM Application to Masonry Arch Bridge Case Studies

Nicolò Damiani[i], Alessia Furiosi[ii], Maria Rota[iii], and Andrea Penna[iv]

ABSTRACT

Thousands of masonry arch bridges are still in operation today, forming a vital part of the railway and road networks in Italy and Europe. As most of these bridges were built over a century ago, issues such as material deterioration, lack of maintenance, as well as increased axle loads and traffic volumes have raised concerns about their long-term structural integrity. In earthquake-prone regions, the integrity of these structures is also challenged by loads induced by seismic activity. Within this context, an increasing number of existing masonry bridges in Italy have been incorporated into the national Seismic Observatory of Structures. This initiative aims to monitor oscillations caused by earthquakes, providing the technical and scientific community with fundamental data to understand the seismic response of these structures. This paper presents three-dimensional models of two existing masonry arch bridges, developed using an advanced modeling strategy based on the discrete element method. Located in Northern and Southern Italy, these bridges are constructed from regular stone masonry and are characterized by multiple consecutive arch vaults. The complete bridge structures are modeled as assemblies of discrete blocks, incorporating all structural and non-structural components, such as piers, abutments, arch vaults, spandrel walls, and backfill material. The geometric characteristics of the bridges and mechanical properties of the materials were assigned based on available in-situ surveys. The numerical dynamic behavior of the generated models is compared and validated against monitoring data collected from these structures, also investigating the effects of alternative boundary conditions at the bridge extremities. Nonlinear time-history simulations with different seismic inputs are then conducted to assess the bridge vulnerability and identify critical structural areas, guiding the design of potential retrofit interventions to enhance their seismic performance.

KEYWORDS

Boundary conditions, Distinct element method, Masonry arch bridge, Structural monitoring, Nonlinear dynamic analysis

[i] Postdoctoral Researcher, Department of Civil Engineering and Architecture (DICAr), University of Pavia, Pavia, Italy, nicolo.damiani@unipv.it
[ii] Ph.D. Candidate, Department of Civil Engineering and Architecture (DICAr), University of Pavia, Pavia, Italy, alessia.furiosi01@universitadipavia.it
[iii] Researcher, European Centre for Training and Research in Earthquake Engineering (EUCENTRE), Pavia, Italy, maria.rota@eucentre.it
[iv] Full Professor, Department of Civil Engineering and Architecture (DICAr), University of Pavia, Pavia, Italy, andrea.penna@unipv.it

INTRODUCTION

A significant number of masonry arch bridges in Italy and Europe were constructed over a century ago, preceding the widespread adoption of modern materials such as steel and reinforced concrete, which gained prominence in the first half of the 20th century. Despite their age, these structures remain vital components of road and rail networks, acting as both engineering landmarks and enduring symbols of architectural heritage [1],[2]. Their integrity and structural stability are challenged by various loading conditions, including seismic actions. Recent seismic events caused localized damage in masonry arch bridges, including cracking, residual deformations, and in some cases, collapses. Notable weaknesses include the out-of-plane overturning of spandrel walls and the formation of hinges within the arch vaults, which can compromise bridge structural integrity and functional performance [3]. Several structures, including masonry arch bridges, have been incorporated into the National Seismic Observatory of Structures (OSS) of the Italian Department of Civil Protection. Monitoring these structures provides valuable experimental data for the development of numerical models to study their behavior. Masonry arch bridges have been analyzed in the literature using various modeling strategies. Traditionally, limit analysis has been employed to assess the stability of masonry arches, offering a simplified approach with low computational demands [4]. However, accurately capturing the static and the dynamic behavior of these structures, necessitates more sophisticated modeling techniques, such as finite element analysis [5]. However, these models are limited to scenarios with negligible relative movement between masonry units. Discontinuum-based models have proven highly effective in accurately simulating the response of masonry structures, such as arch bridges, overcoming these limitations [7]-[10] In this study, discontinuum models inspired by two existing Italian masonry arch bridges are developed. The numerical dynamic behavior of the bridges is validated and compared with experimental data from structural monitoring in terms of vibration modes and periods. Finally, nonlinear time-history analyses (NLTHA) are performed using a set of seven two-component ground-motion records, as recommended by the Italian building code [11].

DISCONTINUUM MODELING OF MASONRY ARCH BRIDGES

Numerical modeling framework

This study employs a numerical approach based on the Distinct Element Method (DEM) to simulate the behavior of masonry structures. DEM is particularly well-suited for analyzing masonry, as it accurately represents the discrete nature of the material by modeling it as an assembly of discrete blocks, capturing block separation, large relative movements, rotations, and the automatic detection of joined and non-joined blocks [12]. In this work, the commercial software 3DEC was employed [13], adopting a mixed modeling strategy to simulate the three-dimensional response of the studied bridges, as shown in Figure 1.

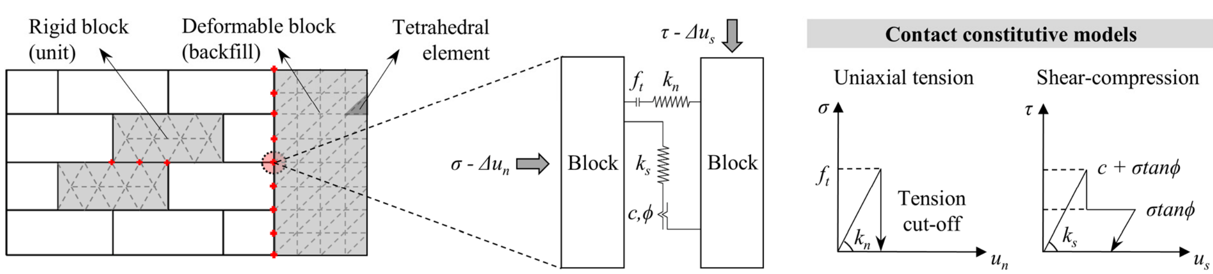

Figure 1: Adopted DEM modeling strategy and contact constitutive laws

In particular, masonry units, constituting piers, abutments, arches, and spandrel walls, were modeled as rigid blocks with six degrees of freedom. Interfaces (or contacts) between adjacent blocks were represented by zero-thickness spring layers with normal and shear stiffnesses (k_n, k_s). The contact shear behavior was modeled using a Mohr-Coulomb slip model, defined by cohesion (c) and friction angle (ϕ). The contact normal behavior was controlled by a finite tensile strength (f_t) with tension cut-off, while compressive failure was not admitted. On the other hand, the backfill material was modeled as a continuum single deformable block [14]. This deformable block was then discretized into multiple tetrahedral elements, and its constitutive behavior was described by a Mohr-Coulomb plasticity model with tension cut-off.

In 3DEC, a dynamic time-integration algorithm is employed to solve the equations of motion for each block, using an explicit finite difference method [13]. A size scaling-technique was iteratively applied to achieve an optimal balance between computational efficiency and accuracy of the numerical outcomes.

Overview of the selected case studies

This study investigates the behavior of two vehicular masonry arch bridges, whose models were inspired by two existing 19th-century Italian bridges. The first case study is based on the S. Chiara bridge (Figure 2), located between Noto and Palazzolo in Southern Italy, and will be referred to in the following as CS1. The structure consists of four consecutive arch vaults, each with an approximate span of 10.0 m. The total length of the bridge is 62.0 m, and its transverse dimension measures approximately 7.1 m. The bridge structure consists of two abutments and three piers, built with ashlar masonry with loose rubble infill. They exhibit semicircular profiles and have a total height of 9.5 m. The masonry consists of squared stone units with average dimensions of 60 × 50 × 45 cm, arranged in a stretcher-bond pattern. In-situ surveys indicated a uniform thickness of 45 cm for spandrel walls along their height. A 120-cm-high, 35-cm-thick masonry parapet, bonded to the spandrel wall below, completes the bridge structure. In-situ core drillings revealed a backfill material made of loose coarse material, covering arch barrels, piers and abutments.

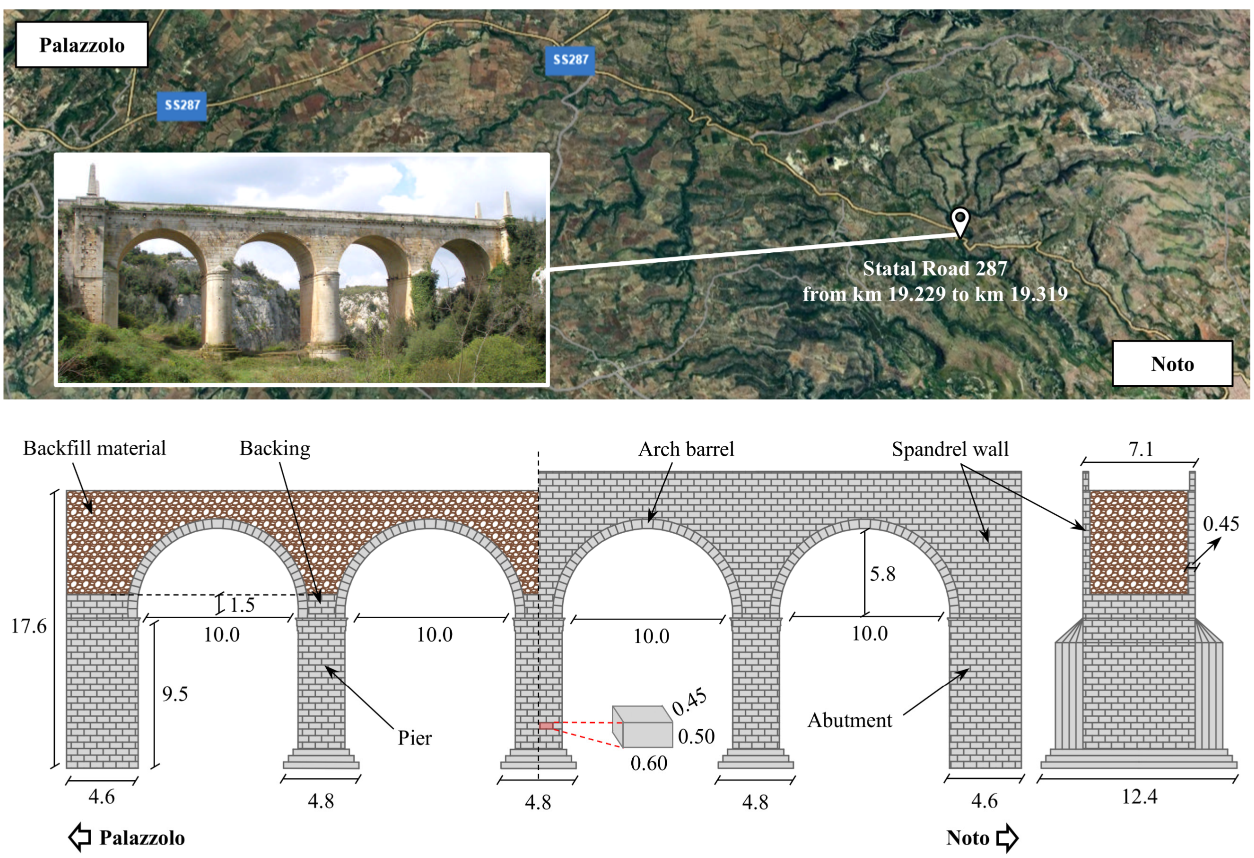

Figure 2: Location and scheme of the bridge structure (CS1). Units of meters

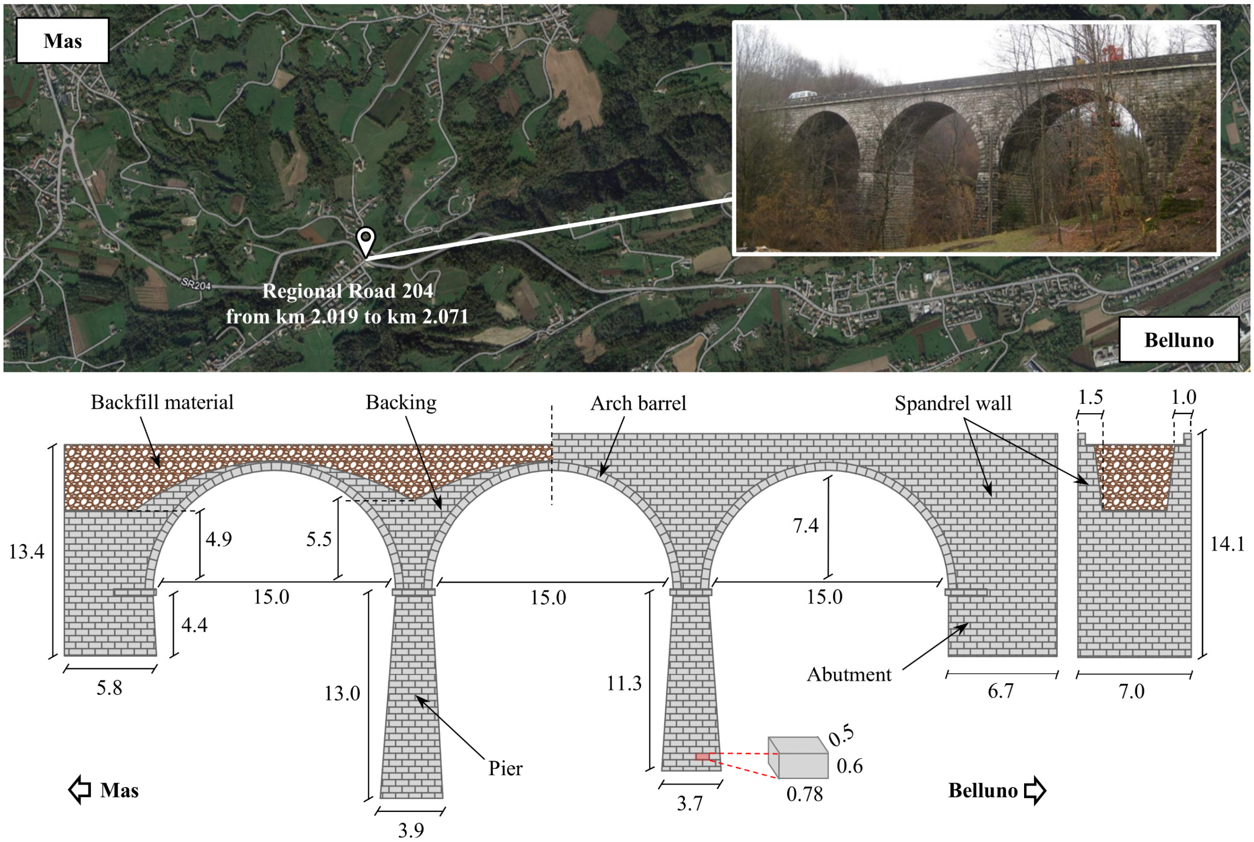

Figure 3: Location and scheme of the bridge structure (CS2). Units of meters [10]

The second case study is based on the bridge spanning the Gresal stream in Northern Italy (Figure 3), which connects the cities of Belluno and Mas, and will be referred to as CS2. The bridge, characterized by three sequential arch vaults, spans a total length of 67.0 m and has a transverse width of 7.0 m. Each arch vault covers an average span of approximately 15.0 m. The bridge structure comprises two abutments and two piers, exhibiting a tapered geometry with heights of 13.0 meters and 11.3 meters, respectively. The masonry is constructed from soft stone (calcarenite) blocks with average dimensions of 78 × 60 × 50 cm, arranged in a stretcher-bond pattern. In-situ core drilling revealed a backing layer made of masonry stone covering the arch barrels, with a backfill made of loose coarse material above. Due to the lack of data on the thickness of the spandrel walls, its variation in height, and the resulting backfill geometry, these walls were assumed to be tapered, with thickness ranging from 1.5 m at the base to 1.0 m at the top [10].

Discrete model details and assigned mechanical properties

In both case studies, masonry was modeled using rigid blocks with zero-thickness joints, while backfill was represented as a single deformable block. For CS1 model, different block dimensions were selected for each structural component to balance model accuracy, computational efficiency, as well as to facilitate model generation. For the arch vaults, 60 × 50 × 45 cm blocks were used, while slightly larger blocks, with dimensions 75 × 70 × 45 cm, were employed for backing and spandrel walls. To further optimize the model, the loose infill of piers and abutments was represented using 75 × 70 × 45 cm rigid blocks with proper contact stiffnesses. For the outer masonry leaf of piers and abutments, blocks with a height of 80 cm, a width of 70 cm, and alternating thicknesses of 20 cm and 60 cm were used in each course to accurately represent the masonry bonding observed in the surveys. The bridge was supported by four fixed rigid blocks placed at the base of each pier and abutment, highlighted in red in Figure 4.

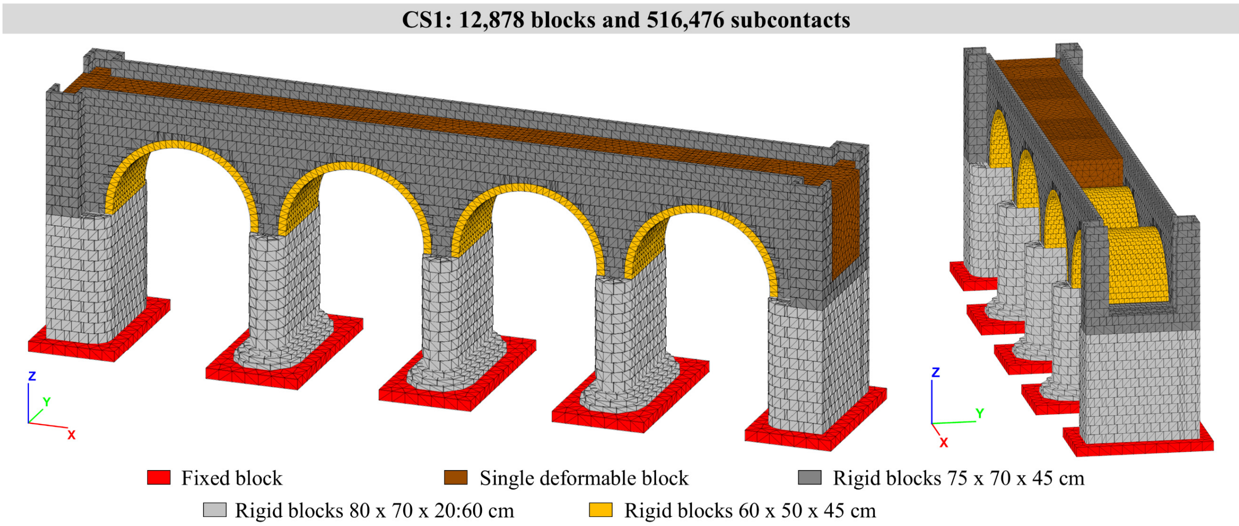

Figure 4: Three-dimensional discrete model of CS1

For CS2 model, the number of blocks was properly reduced by employing larger block dimensions compared to the existing masonry units. This approach aimed at minimizing computational demand while maintaining accuracy in the final results. Specifically, for the three arch vaults, representing the most critical structural elements, blocks with real dimensions (78 × 60 × 50 cm) were employed. Differently, for the remaining masonry components, including piers, abutments, spandrel walls, and backing, larger blocks with doubled dimensions (156 × 120 × 100 cm) were used as summarized in Figure 5. Also in this case, the bridge was supported by four fixed rigid blocks at the base of each pier and abutment.

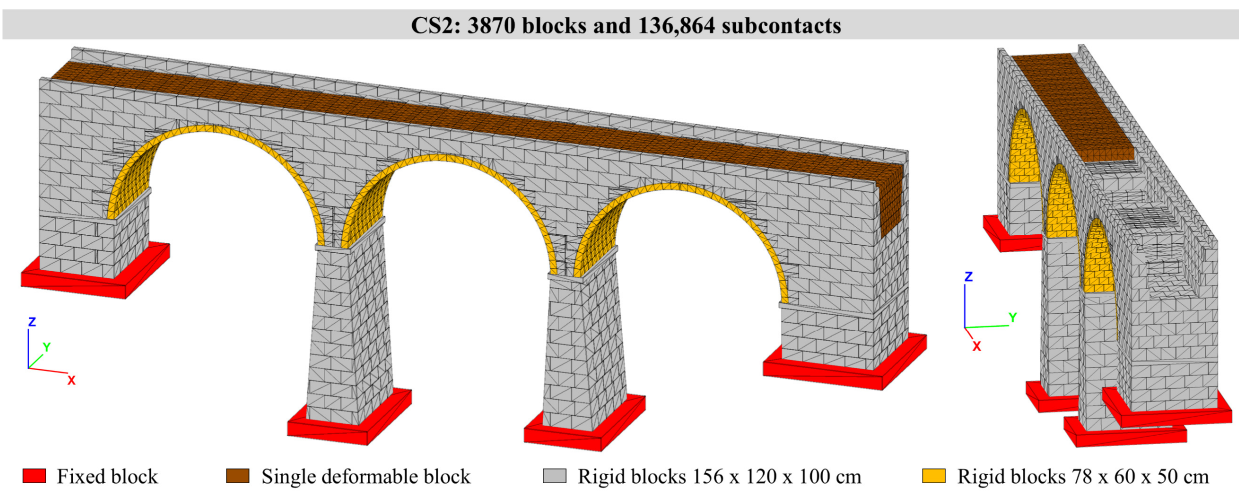

Figure 5: Three-dimensional discrete model of CS2

Regarding the mechanical properties of the materials, apart from in-situ core drillings used to determine the type of masonry units and reconstruct the stratigraphy of the studied bridges, no characterization tests were performed on the collected materials. Therefore, the mechanical properties of masonry assigned in the models, including density (ρ), elastic modulus (E), shear modulus (G), tensile strength (f_t) cohesion (c), and friction angle (ϕ), were estimated based on the values suggested by the Italian norms [11] for existing ashlar natural-stone regular masonry (CS1) and existing soft-stone regular masonry (CS2). Due to the lack of data, the backfill mechanical properties assigned to the Mohr-Coulomb plasticity model were determined based on the recommendations of recent studies [14]. The backfill deformable block was discretized into multiple tetrahedral elements with a maximum edge length of 0.5 m. All the assumed values are listed in Table 1.

Table 1: Mechanical properties of masonry and backfill material [10],[11],[14]

Case study	Element	ρ [kg/m^3]	E [MPa]	G [MPa]	f_t [MPa]	c [MPa]	ϕ [°]
CS1	Arch vaults, piers, abutments, spandrel walls, backing	1722	4000	1600	0.10	0.18	30
	Piers and abutments filling material	1524	1000	400	0	0.02	40
	Backfill material	1500	400	160	0	0.02	40
CS2	Piers, abutments, spandrel walls, backing	1600	1410	450	0.10	0.15	30
	Arch vaults	1600	1692	540	0.10	0.15	30
	Backfill material	1600	100	42	0	0.02	40

The use of rigid blocks with varying dimensions required the calculation of joint stiffness values for each contact typology. Based on the assumed masonry elastic and shear moduli (E_m, G_m), the normal and shear joint stiffnesses were determined as $k_n = E_m / d_c$ and $k_s = G_m / d_c$, where d_c represents the centroid-to-centroid distance between adjacent blocks. Note that for contacts between blocks with different dimensions, an average value of d_c was employed. To model the interaction between the masonry and the backfill, spring layers were introduced with a stiffness value reduced to 20% of that assigned to the piers, abutments, and spandrel walls. Moreover, the contacts between masonry rigid blocks and backfill deformable block were assumed to have zero tension, zero cohesion, and a friction angle of 35° [10]. The contact stiffness values assigned in both models are summarized in Table 2. Note that only the values related to the main contacts are listed, as all remaining values can be directly derived from those provided.

Table 2: Normal and shear stiffness values assigned to the joints in the models.

Case study	Type of contact	k_n [MPa/m]	k_s [MPa/m]
CS1	Masonry arch vaults	8890	3560
	Masonry backing and spandrel walls	5520	2210
	Masonry piers and abutments	5310	2120
	Piers and abutments filling material	1330	531
CS2	Masonry piers, abutments and spandrel walls	1150	368
	Masonry arch vaults	2740	876

EIGENVALUE ANALYSIS AND INFLUENCE OF BOUNDARY CONDITIONS

This research investigated the influence of different boundary conditions on the dynamic response of the selected bridges. The presence of surrounding soil and structural portions not directly included in the developed models, particularly near the abutments, makes it challenging to define appropriate boundary conditions. Given the availability of structural monitoring data, this aspect is especially relevant for accurately characterizing the bridge response and gaining valuable insights into how boundary conditions should be treated in such structures. Two alternative boundary conditions were considered for both case studies: laterally free abutments (CS1-F and CS2-F) and laterally restrained abutments (CS1-R and CS2-R). For the restrained abutment models, compared to the models shown in Figure 4 and Figure 5, two additional blocks were introduced at the abutment extremities along their height to restrict displacements in the *x*- and *y*-directions within the bridge plane. The stiffness values assigned to the interfaces between these blocks and the other bridge components were iteratively calibrated, with a final adopted value set at 50% of the stiffness of the adjacent material (i.e., masonry or backfill).

To preliminarily assess the dynamic behavior of the bridges, an eigenvalue analysis was performed using the software 3DEC, which employs a power iteration method to compute modal frequencies [13]. Within the 3DEC environment, eigenvalue analyses are restricted to models composed of a single block type: either rigid or deformable. To enable the analysis, the deformable backfill block was replaced with an assembly of rigid rectangular blocks, with equivalent stiffnesses assigned to their interfaces. Specifically, for CS1 models, 70 x 45 x 40 cm blocks were employed, with contact stiffnesses k_n = 1330 MPa/m and k_s = 531 MPa/m, determined as previously described. Similarly, for CS2 models, 156 x 120 x 100 cm blocks were utilized, with contact stiffnesses k_n = 7700 MPa/m and k_s = 3100 MPa/m.

Figure 6 displays the shapes of the first three fundamental vibration modes and the associated periods for the first case study. For CS1-F, the first mode ($T_{1,CS1-F}$ = 0.57 s) is characterized by predominant longitudinal bending of the bridge, the second mode ($T_{2,CS1-F}$ = 0.51 s) exhibits transverse bending, and the third mode ($T_{3,CS1-F}$ = 0.43 s) corresponds to a higher-order transverse bending mode. However, the obtained mode shapes and periods were not consistent with the structural monitoring data available for this case study (Figure 6). Conversely, the CS2-R results exhibit a stiffer response in both structural directions, with mode shapes and vibration periods that closely match the monitored data. Specifically, the first mode ($T_{1,CS1-R}$ = 0.32 s) is dominated by transverse bending of the bridge, the second mode ($T_{2,CS1-R}$ = 0.21 s) represents a second-order transverse bending mode, and the third mode ($T_{3,CS1-R}$ = 0.18 s) corresponds to longitudinal bending. These results highlight the importance of accurately defining boundary conditions at the bridge extremities to ensure reliable dynamic response predictions.

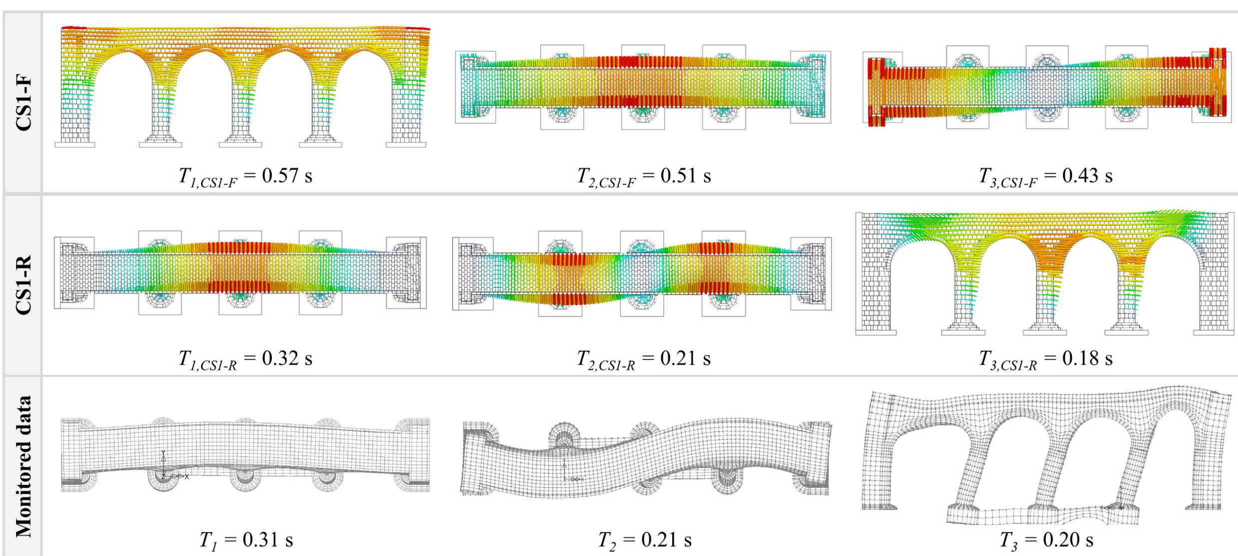

Figure 6: Eigenvalue analysis results for CS1-F and CS1-R and experimental data

In Figure 7, the mode shapes and periods for CS2-F and CS2-R are illustrated. For the free abutments case, the first mode ($T_{1,CS2-F}$ = 0.69 s) is characterized by predominant transverse bending of the bridge, the second mode ($T_{2,CS2-F}$ = 0.48 s) corresponds to longitudinal bending, and the third mode ($T_{3,CS2-F}$ = 0.42 s) represents a second-order transverse bending mode. Unlike the first case study, no structural monitoring data were available for this bridge. Instead, the obtained results were validated against those from a FEM model based on the same modeling assumptions [10]. Consequently, for the CS2-R model, the same assumptions adopted for the calibrated CS1-R model were adopted. By laterally restraining the abutments, the structure exhibits increased stiffness resulting in reduced vibration periods, similar to CS1-R. Specifically, for CS2-R, the first mode ($T_{1,CS2\text{-}R}$ = 0.57 s) exhibits transverse bending, the second mode ($T_{2,CS2\text{-}R}$ = 0.30 s) corresponds to a second-order transverse bending mode, and the third mode ($T_{3,CS2\text{-}R}$ = 0.24 s) is characterized by longitudinal bending.

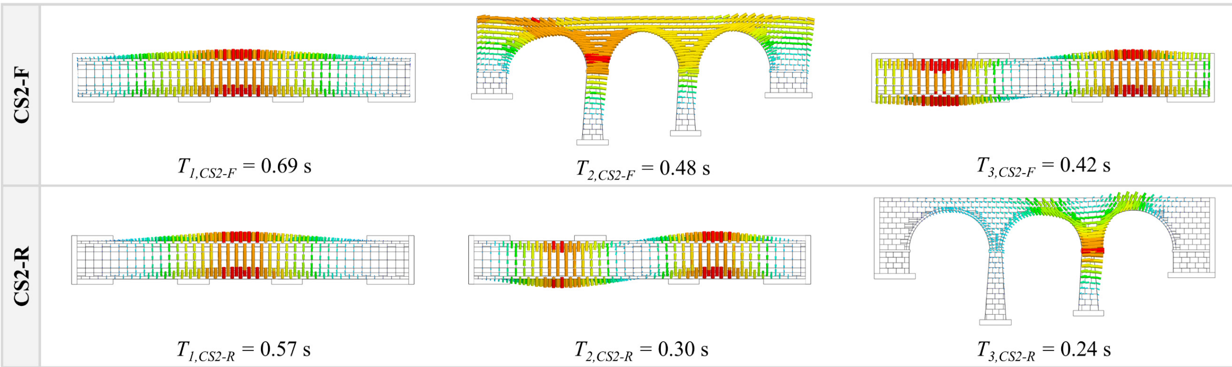

Figure 7: Eigenvalue analysis results for CS2-F and CS2-R

DYNAMIC RESPONSE SIMULATIONS

Nonlinear time-history analyses (NLTHAs) were carried out on both case studies, considering two different boundary conditions. The main objective was to evaluate how variations in these conditions might influence the seismic response of masonry arch bridges.

Ground-motion record selection

Seven three-component ground-motion records were selected according to the Italian building code [11] for the ultimate limit state (10% probability of exceedance in 50 years, corresponding to a 475-year return period). The site in L'Aquila, classified as soil type D, use class III, and topographic category T1 [11], was selected as representative of potential Italian seismicity, enabling the evaluation of structural performance under generalized seismic ground motions. In addition, the structure fundamental periods ($T_{1,CS1\text{-}F}$, $T_{1,CS1\text{-}R}$, $T_{1,CS2\text{-}F}$, $T_{1,CS2\text{-}R}$) were considered to ensure the selected records met the spectrum compatibility over a period range from 0.15 s to 1.2 s (twice the maximum fundamental period), ensuring that in this range the mean elastic spectrum of the two components aligns with the target spectrum within a 90-130% tolerance. Figure 8a and Figure 8b present the acceleration response spectra of these seven records, along with their peak ground acceleration (*PGA*), peak ground velocity (*PGV*), and significant duration ($D_{5\text{-}95}$).

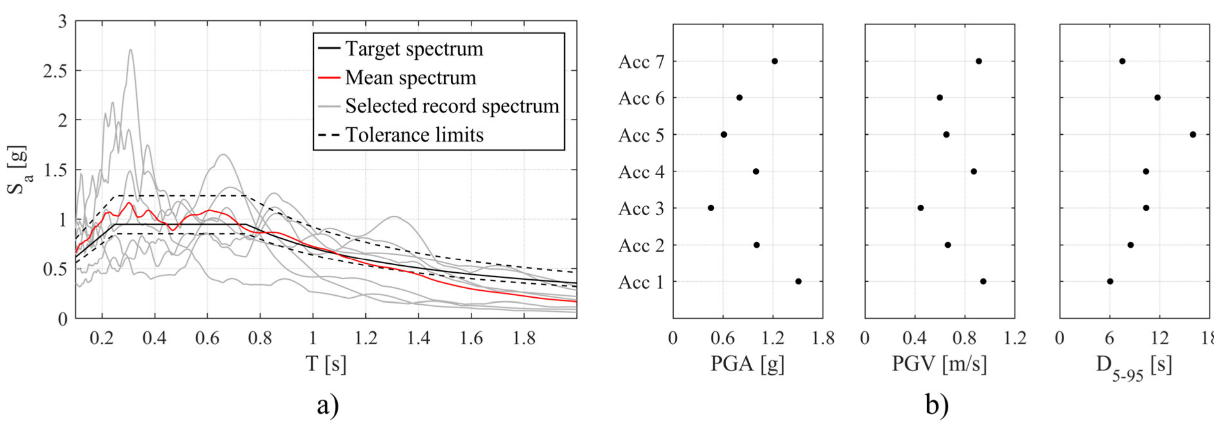

Figure 8: a) Target and selected ground-motion spectra; b) *PGA*, *PGV*, and $D_{5\text{-}95}$

To address the well-known limitations associated with classical Rayleigh damping when using 3DEC, a three-component Maxwell damping model was employed [10]. A 2% viscous damping ratio was applied within a frequency range of 0.5–12 Hz, covering the first and third natural frequencies of the studied structures as well as the dominant frequencies of the input motions [13][15].

Numerical results

This section presents the most significant results from the performed nonlinear time-history analyses (NLTHA), illustrating the damage patterns obtained under seven seismic ground-motion records for the four modeled configurations. In both case studies, the models with free abutments exhibited progressively greater and more widespread damage than those with restrained abutments. Under free abutment conditions, damage was predominantly concentrated in the spandrel walls above the abutments, where an out-of-plane overturning mechanism was triggered. By contrast, the restrained abutment condition largely prevented this mechanism, resulting in more severe damage to the piers, although minor out-of-plane deflections of the spandrel walls were observed.

Figure 9 illustrates the final damage patterns following the application of the most critical ground-motion record. In the figure, a displacement amplification factor of 2 was applied to the deformed shapes to enhance visualization, while the backfill material was omitted. In both case studies, the free abutment configuration showed larger relative block displacements (indicating the magnitude of masonry cracking). Moreover, CS2 generally experienced lower block displacements than CS1 under both boundary conditions. In CS1-F, out-of-plane overturning of the spandrel walls above piers and abutments was observed, along with minor damage to the arch vaults. The restrained boundary conditions at the abutments resulted in CS1-R model in a reduction of the out-of-plane deflection of the spandrel walls, resulting in minor damage to the arch vaults. In CS2-F, localized damage was observed in the spandrel walls above the abutments, where the out-of-plane overturning mechanism initiated, leading to minor damage in the arch vaults. Conversely, in CS2-R, the damage was mainly concentrated in the piers, while the out-of-plane overturning of the spandrel walls was less pronounced, especially above the abutments.

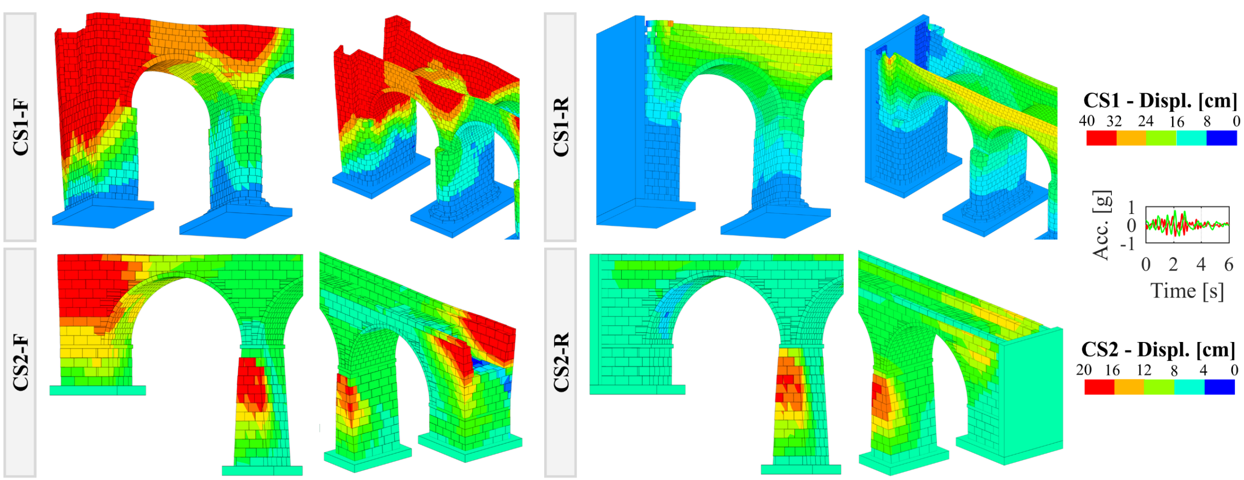

Figure 9: Numerical outcomes illustrating damage patterns for a selected record.

Figure 10, presents the relationship between the peak ground acceleration (PGA) of the applied two-component records and the maximum relative displacements of the most vulnerable bridge components, namely the arch vaults and spandrel walls, for each performed analysis. Note that the maximum relative displacements are reported as mean values obtained for the arch keystones and for each spandrel wall above every pier and abutment, considering both the front and back sides of the bridge. The response of the arch vaults was assessed in the longitudinal direction (x-axis), whereas the transverse direction (y-axis) was considered for the spandrel walls, due to their susceptibility to out-of-plane deformations.

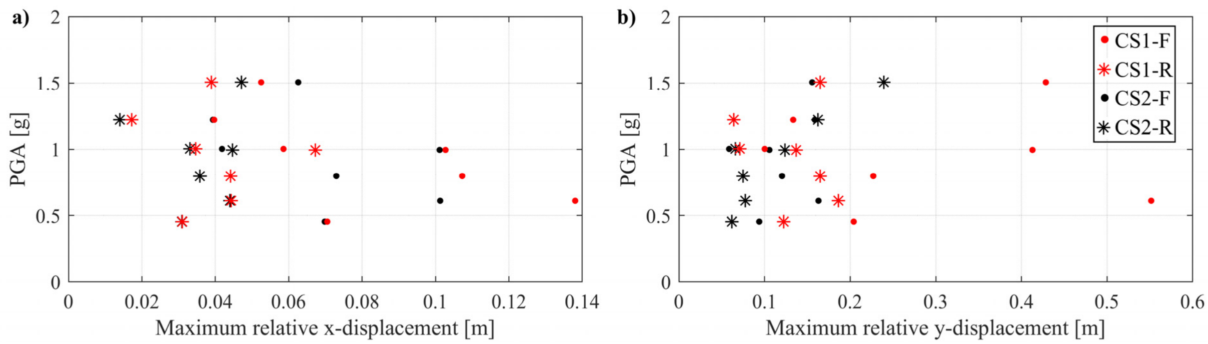

Figure 10: Bridge response in terms of PGA and maximum relative displacements: a) arch vault keystones; b) spandrel walls.

Figure 10a shows that the restrained boundary conditions effectively reduced longitudinal displacements in the arch vaults for both case studies, mitigating hinge formation and potential loss of equilibrium. Figure 10b reveals that, in the case of CS1, the spandrel wall displacements under both laterally free (CS1-F) and laterally restrained (CS1-R) conditions were significantly higher than those observed in CS2, primarily due to the higher slenderness of CS1 spandrel walls. Moreover, the implementation of restrained conditions substantially decreased out-of-plane displacements in CS1 model, with CS1-R exhibiting up to a twofold reduction in transverse displacements compared to CS1-F.

From a vulnerability assessment standpoint (e.g., fragility curve generation), the selection of an appropriate engineering demand parameter (EDP) is crucial. Although arch vault damage was shown to be a suitable EDP for CS2 [10], it may not adequately represent the global damage state in CS1, given the potential difference in damage mechanisms. Indeed, an EDP more directly tied to the out-of-plane response of the spandrel walls would be more appropriate. Future studies should further investigate these aspects to identify the most representative EDP as bridge geometry and structural details vary.

CONCLUSIONS

This paper presented a numerical study on the dynamic response of two masonry arch bridges inspired by real structures located in Italy, employing the Distinct Element Method (DEM). Two three-dimensional models were developed using both rigid and deformable blocks, incorporating structural and non-structural components. The masonry was represented as an assembly of rigid blocks with zero-thickness interfaces behaving according to a Mohr-Colomb contact model, while the backfill material was modeled as a single deformable block with a Mohr-Coulomb plasticity model. The dynamic response of the two case studies was investigated under the influence of different boundary conditions. Specifically, for each case study, two boundary conditions were examined: one considering the abutments as free and the other assuming them as restrained. To study the influence of boundary conditions, an eigenvalue analysis was performed, and its outcomes were compared with available data from structural monitoring. The dynamic behavior of the two case studies was finally assessed through nonlinear time-history analyses, applying seven two-component ground motion records, as recommended by the Italian building code. The research presented in this paper is only a part of an ongoing research project related to existing masonry arch bridges. Further dynamic analyses, applying 200 three-component ground-motion records, are currently underway to gain a more comprehensive understanding of bridge dynamic behavior and seismic vulnerability. The extensive database generated using DEM will facilitate the assessment of bridge response and progressive damage under various input signals, aiding in the identification of different limit states. The assessment of the seismic vulnerability of the case-study bridges might allow studying the effectiveness of potential retrofit solutions.

ACKNOWLEDGEMENTS

The presented study was partly developed within the activities of the 2022-23 and 2024-26 ReLUIS-DPC and EUCENTRE-DPC research programs, funded by the Italian National Department of Civil Protection (DPC). The opinions and conclusions expressed by the authors do not necessarily reflect those of the funding entity. The authors express their gratitude to the Itasca Educational Partnership (IEP) Program and Harpaceas S.R.L. The valuable advice of Prof. A. Brencich (University of Genoa) is also gratefully acknowledged, along with the fruitful collaboration of the research group led by Prof. F. da Porto (University of Padua).

REFERENCES

[1] Union Internationale des Chemins de Fer (1994). *Charges à Prendre en Considération Dans le Calcul des Ponts-Rails*. UIC Code 776-1R.

[2] Page, J. (1993). *Masonry Arch Bridges*. HMSO.

[3] Oliveira, D.V., Lourenço, P.B. and Lemos, C. (2010) "Geometric issues and ultimate load capacity of masonry arch bridges from the northwest Iberian Peninsula." *Engineering Structures,* 32(12), 3955-3965.

[4] Heyman, J. (1995). *The Stone Skeleton: Structural Engineering of Masonry Architecture*. Cambridge University Press.

[5] Manzini, C.F., Morandi, P., Borzi, B., Iodice, F., Mauro, A., Vecchi, A. and Iacobini, F. (2022). "Derivation of Fragility Curves for the Seismic Vulnerability Assessment of Railway Masonry Arch Bridges." *Proceedings of the 1st Conference of the European Association on Quality Control of Bridges and Structures*, 893-902.

[6] Malomo, D. and DeJong, M.J. (2022). "A Macro-Distinct Element Model (M-DEM) for simulating in-plane/out-of-plane interaction and combined failure mechanisms of unreinforced masonry structures." *Earthquake Engineering & Structural Dynamics,* 51(4), 793-811. doi:10.1002/eqe.3591

[7] McInerney, J. and DeJong, M.J. (2015). "Discrete element modeling of groin vault displacement capacity." *International Journal of Architectural Heritage*, 9(8), 1037-1049.

[8] Oktiovan, Y., Davis, L., Wilson, R., Dell'Endice, A., Mehrotra, A., Pulatsu, B. and Malomo, D. (2024). "Simplified Micro-Modeling of a Masonry Cross-Vault for Seismic Assessment Using the Distinct Element Method." *International Journal of Architectural Heritage,* 18(12), 1915-1948.

[9] Sarhosis, V., Forgács, T. and Lemos, J.V. (2020). "Modelling Backfill in Masonry Arch Bridges: A DEM Approach." *Proceedings of ARCH 2019*, 178-184. doi:10.1007/978-3-030-29227-0_16

[10] Furiosi, A., Damiani, N., Rota, M. and Penna, A. (2025) "Seismic fragility assessment of a multi-span masonry arch bridge using a discontinuum modeling approach." *Earthquake Engineering & Structural Dynamics*. Submitted in January 2025.

[11] MIT. Decreto Ministeriale 17 gennaio 2018: Aggiornamento delle Norme tecniche per le costruzioni. Ministero delle Infrastrutture e dei Trasporti, Rome, Italy (in Italian).

[12] Cundall, P.A. (1971). "A computer model for simulating progressive, large-scale movement in blocky rock system." *Proceedings of the International Symposium on Rock Mechanics*, Vol 8, 129-136.

[13] Itasca Consulting Group Inc (2024). *3DEC Three Dimensional Distinct Element Code, Itasca Software 9.2 documentation.* https://docs.itascacg.com/itasca920/3dec/docproject/source/3dechome.html

[14] Pulatsu, B., Erdogmus, E. and Lourenço, P.B. (2019) "Simulation of masonry arch bridges using 3D discrete element modeling." *Structural Analysis of Historical Constructions: An Interdisciplinary Approach*, 871-880.

[15] Dawson, E.M. and Cheng, Z. (2021). "Maxwell Damping: An Alternative to Rayleigh Damping." *Geo-Congress 2021*, 34-45.